Supplementary Materials and Methods 1

Temperature and relative humidity

Measurements during the experiment

For the experiment, we used a logger (BL-30, Trotec GmbH, Heinsberg, Germany) that measured temperature and relative humidity of the ambient air. In the container experiments, it was placed close to the containers. Control measurements, however, revealed that the measured relative humidity and temperature of the room is the lower boundary of the values inside the containers: internal relative humidity was ~75% due to the water supply. Assuming that mean temperature inside the vials was 2 °C higher than the measured room temperature during the day (due to the lamps) and identical during the night, and assuming a lifetime of 60 days, this converts into 60 Kd (7%) offset of physiological age for temperatures ca. 15 °C above the threshold (i.e. ca. 26 °C). For the free-flight experiment, the values measured next to the cage corresponds well to the values inside the cage for both humidity and temperature. Temperature and illuminance were also measured outdoors and inside the setups to allow further comparisons. Temperature, relative humidity and illuminance was 24.7±2.8 °C, 38±6% and 380-840 lx in container experiments and 24.1±0.8 °C, 41±7% and 350-42000 lx in free flight experiments, respectively. Measurements outside were done on days with temperatures between 19 °C and 26 °C and illuminances between 6000 lx and 120 000 lx.

Estimation of the physiological age

Temperature influences the activity and metabolism of a fly. We thus used physiological age (Skovgård and Nachman, 2004) instead of age. Temperature was recorded during 63-73% of the experimental time. To continuously estimate physiological age, we thus derived temperature means for each light and dark period and interpolated missing data using weighted linear regression (Fig. S1). In containers, this interpolation assumed t_0=0 min on midnight (00:00:00) on July 21th, 2018 (activity experiment), and midnight (00:00:00) on April 20th, 2018 (free-flight experiment). For container experiments, the linear equations was $T(t)=at+b$ (with a = -2.617×10^{-3} °Ch^{-1} and b = 29.87 °C for day temperatures; adjusted R^2 = 0.911; and a = -2.373×10^{-3} °Ch^{-1} and b = 28.79 °C for night temperatures; adjusted R^2 = 0.942). In flight cage experiments, the coefficients were a = 0.1002×10^{-3} °Ch^{-1} and b = 24.52 °C for day temperatures (adjusted R^2 = -0.0145), and a = 0.2453×10^{-3} °Ch^{-1} and b = 23.34 °C for night temperatures (adjusted R^2 = 0.0006). For the temperature integral, we used our estimated means for each light/dark cycle and for physiological age estimation a reference temperature of 11 °C (Skovgård and Nachman, 2004). Figure S2A, B shows the relationship between chronological and physiological age for all tested flies. In the container experiment, different cohorts were started at different times as shown by different colours. In flight experiment, we tested only one cohort of flies. Survivorship plots for both age measures are shown for container experiment in figure S2C-F and for flight experiment in figure S2G, H.

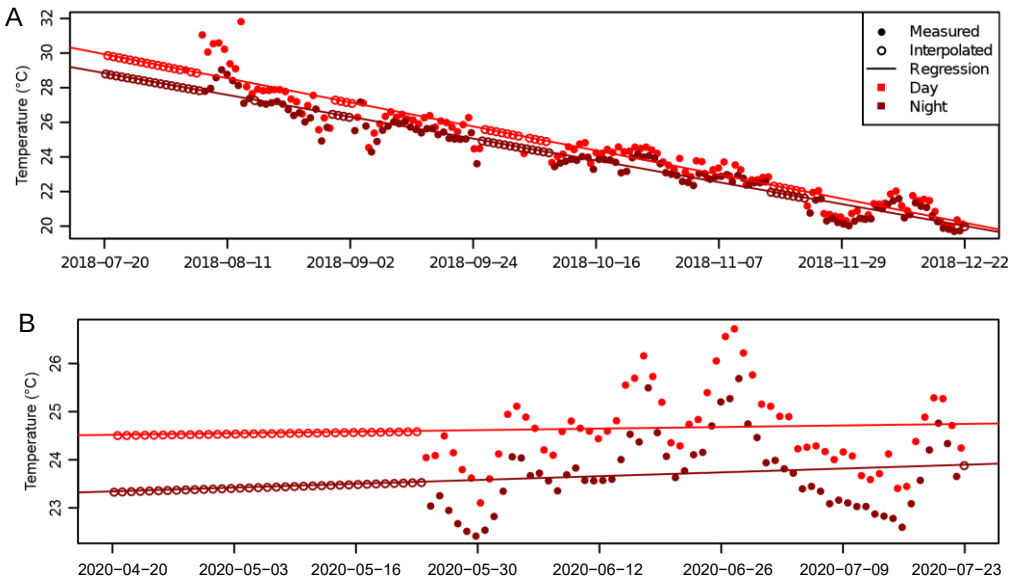

Fig. S1. Measured (filled circles) and interpolated/extrapolated (open circles) temperature data for each day (light red) and night (dark red) section for (A) container and (B) flight cage experiments. Lines, linear regression fit. X-scale shows date.

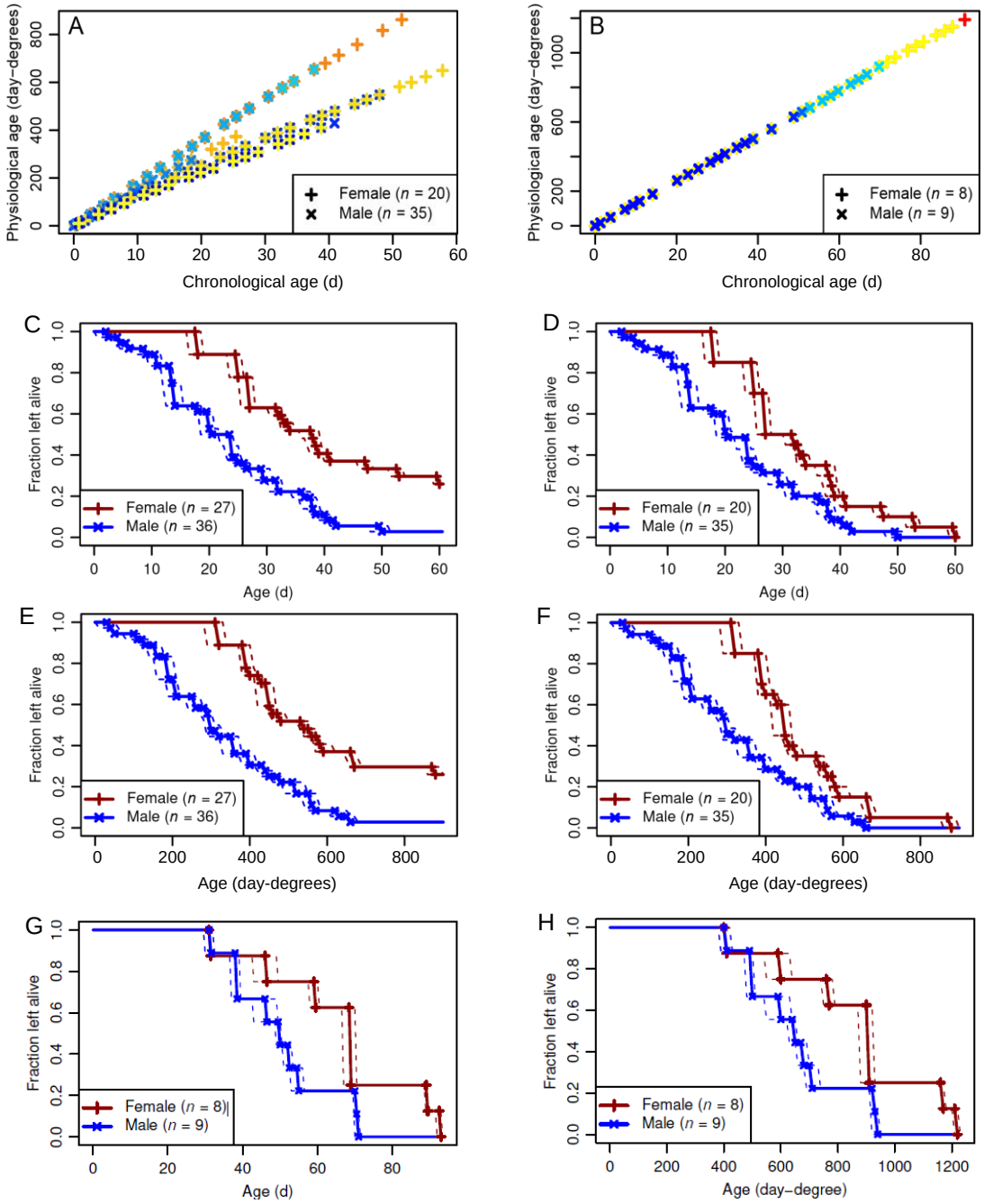

Fig. S2. Age comparison and mortality. (A, B) Physiological compared to chronological age for container in *A* and flight cage experiments in *B*. We tested several groups (cohorts), thus data overlap (see text S1). (C-F) Mortality of flies in container experiment for chronological age in *C* and *D*, and physiological age in *E* and *F*. *C*, *E*: all experimental flies; *D*, *F*: only those that died during the experimental time (and could therefore be entered into the analysis). Dashed lines show minimum and maximum values. Solid lines indicate means. (G, H) Mortality of flies used in free flight experiment for chronological age in *G* and physiological age in *H*. Dashed lines show minimum and maximum values, solid lines means.

Supplementary Materials and Methods 2

Software

The software used for data analyses and processing is shown in Table S1.

Table S1. List of software used in this study.

Software	Used for	URL/Reference
Fiji	image mask creation	Schindelin et al. (2012)
ffmpeg	video processing	https://ffmpeg.org
ImageMagick	image processing	https://imagemagick.org
MediaHuman	audio resampling	https://mediahuman.com
processing	image analysis	https://processing.org
Python 3.x	sound analysis, image	https://python.org
R	data processing, analysis	https://www.r-project.org R Core Team (2020)
RStudio	GUI for R	https://rstudio.com
R packages		
abind	array manipulation	Plate and Heiberger (2016)
colorRamps	template for colour tables	Keitt (2012)
data.table	data manipulation	Dowle and Srinivasan (2019)
extrafont	using system fonts	Chang (2014)
exifr	extracting EXIF data	Dunnington and Harvey (2019)
imager	image processing	Barthelme (2020)
jpeg	image processing	Urbanek (2019)
lattice	data visualisation	Sarkar (2008)
magick	image processing	Ooms (2020)
minpack.lm	fitting arbitrary functions	Elzhov et al. (2016)
png	image processing	Urbanek (2013a)
rChoiceDialogs	file explorer	Lisovich and Day (2014)
rcompanion	histogram plotting	Mangiafico (2020)
smoothSurv	basis for piecewise functions	Komárek et al. (2005)
stringi	unicode characters	Gagolewski (2020)
tiff	image processing	Urbanek (2013b)
tuneR	sound analysis	Ligges et al. (2018)

Supplementary Materials and Methods 3

Flight activity in container

Validation of flight activity

To validate our software that was developed to detect flight events in the containers, we conducted a control experiment, in which flight was simultaneously filmed by a Nikon D7100 (Tokyo, Japan) and sound recorded by a Tascam-US-16x08 filter unit (TEAC Europe). Filter settings for gain, frequency, and if applicable Q-factor was -12 dB and 1.7 kHz for high range; 9 dB, 450 Hz, and 0.25 for high mid range; and 12 dB, 350 Hz, and 0.25 for low mid range, respectively. In each control experiment, we placed 5-day old flies into a container in groups of four and filmed their activity for 30 minutes. We tested 3 female and 3 male groups. Temperature inside the container varied between 26.3 °C and 28.6 °C. The software algorithm identified 1395 flight bouts, 507 (~36 %) were manually inspected, of which 85 were dismissed. We found that during bouts corresponding to a total of 144 video frames flies did not fly and in bouts corresponding to 2652 frames at least one flying fly. False-positive rate was ~6 %. In ~41 % of the cases, in which the sound software falsely identified flight bouts, a fly was close to the microphone.

Eventually, from the manually inspected bouts, we further scored 153 “flight bouts” from parts of the video where the algorithm had not identified flight activity. These correspond to 6182 video frames. Never was a fly observed to be flying during these bouts. Sometimes flies beat their wings without (any fly) flying, giving an approximate false negative rate of finding purely sitting activity of less than 1 %. We found that most of the time,

only one fly was active at a time (2428 frames). In ~3.6% of the frames two flies were active (224 frames) that apparently stimulated each other (Fig. S3). We also estimated the likelihood of one active fly by random model and compared these data to the recorded signals and from this decided to assume that on overage only one fly is active at any one time during any sound-recorded flight bout.

Supplementary Materials and Methods 4

Validation of wing outline tracing

Wing outline tracing was manually done by hand using a graphics tablet. This approach yielded maximum errors in wing area of ~1.1% when traced by different persons with a median of ~-0.4% (N=33 traced wing outlines), respectively. Having the same person tracing one wing twice resulted in a difference in wing area of about 0.5%. Automatic tracking procedures were not capable of reliably detecting wing shape and orientation.

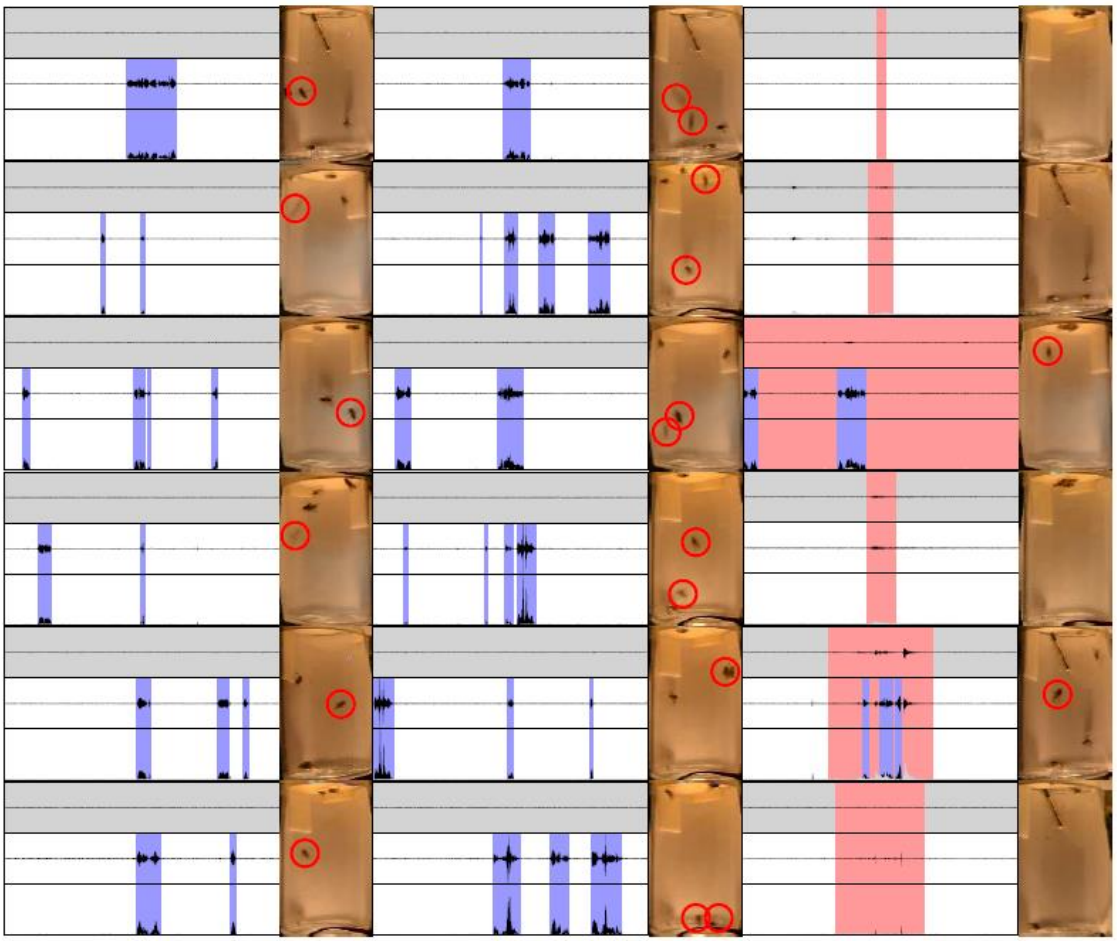

Fig. S3. Validation of flight bout recognition by sound recording. Each example shows five seconds of flight and consists of three horizontal traces and a corresponding photo to the right. The upper trace (background shaded in grey) is the sound signal of the room tone microphone, and the middle trace the sound signal of the microphone of the container. The lower trace shows the bandpass-filtered sound signal. Blue shaded areas indicate flight bouts as found by the sound software. Red shaded areas show an example in which there is external noise not recognised as flight. Red circles in each container indicate flying flies.

Supplementary Materials and Methods 5

Reconstruction of wing root area

The reference wing area is shown in red in figure S4A. We made no attempt to measure the area close to the wing root (P1-P3, Fig. 1B) because this part of the wing mostly stayed intact. Wings were aligned by superimposing the point at the humeral cross-vein (red cross with circle in Fig S4A) and rotating the wing around this point until the crossing between anal vein A_2 and cubitus A_1+CuA_2 was vertically aligned with the pivoting

Journal of Experimental Biology • Supplementary information

point (nomenclature as in McAlpine, 1981). Vein crossings were manually assigned and wing rotation was done using a script written in *R*. A *Python* script turned all wings further around the pivoting point at the humeral cross-vein so as to find the maximum area overlap.

For calculation of moments of wing area, we determined the wings' longitudinal axis. A mean wing root position per experiment and sex was calculated from the initial wing photos. Similarly, a mean direction from root to tip was calculated. These mean values were used for all wings and the tip direction was assumed to stay constant throughout the experiment, even for cases where wing areas were missing. Root position and tip direction (x,y; video pixel) in container experiments was (2368,213)±(15,10), (−0.9858,0.1680)±(0.0031,0.0171) in females, and (2350,211)±(15,9) and (−0.9866,0.1632)±(0.0026,0.0157) in males. In free-flight experiments it was (4629,386)±(15,13) and (−0.9799,0.1995)±(0.0025,0.0121) in females, and (4620,395)±(14,12) and (−0.9822,0.1878)±(0.0029,0.0148) in males. As the area at the wing root (P1-P3, red, Fig. 1A, main text) was not measured, but may influence the value of the second moment of area especially for strongly damaged wings, we added an average "wing root dummy" to the measured wing outline for calculating the area moments. We compared values of area moments between wing outlines without a root dummy (see fig. S4D) and with two different root dummies (a polygon based on the tracked points used for aligning the wings, fig. S4E; and an average wing root -- excluding the alula -- roughly estimated from five photos for each sex in both container and free-flight experiment separately, fig. S4F). As the difference between the two types of dummy was small, we opted for the average traced wing root.

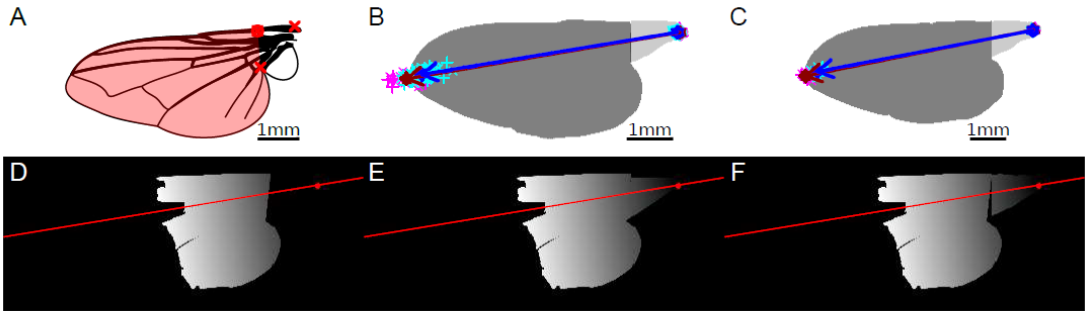

Fig. S4. (A) Schematics showing the traced wing area (red) and points used for alignment of all wings (red crosses). (B,C) Example wing mask (dark grey) with attached standard root (light grey), wing tip and root positions (magenta: single female, dark red: mean female, cyan: single male, blue: mean male) and vectors (longitudinal wing axis) from mean root to mean tip. Drawing in *B* applies to container experiment and in *C* to free-flight experiments in the large flight cage. (D-F) Calculation of the second moment of wing area for a damaged left wing mask of a male fly from the container experiment with mean wing root (red dot) and direction towards wing tip (red line). *D*, traced area only; *E*, polygon root area; *F*, mean root area.

Supplementary Materials and Methods 6

Derivation of equations for A_k and S_k

This section shows how we calculated the 2nd moment of area for one wing from Ellington's (Ellington, 1984b) theoretical framework on two wings. Ellington defined wing area as the total area of both wings:

$$S_{Ellington} = 2\int_0^R c\,d\hat{r}\,, \qquad \text{(eq. S1)}$$

with R the wing length of one wing, $0 \le r \le R$ the position along the wing, and $c(r)$ the wing chord at position r. Area of a single wing is thus:

$$A = \int_0^R c\,dr = \frac{S_{Ellington}}{2} \qquad \text{(eq. S2)}$$

The wings' aspect ratio as introduced by Ellington is defined for both wings as:

$$AR_{Ellington} = \frac{2R}{\bar{c}} = \frac{4R^2}{S_{Ellington}}\,, \qquad \text{(eq. S3)}$$

with mean wing chord:

$$\bar{c} = \frac{A}{R} = \frac{S_{Ellington}}{2R} \qquad \text{(eq. S4)}$$

For a single wing equation S4 may be written as:

$$AR = \frac{R}{\bar{c}} = \frac{R^2}{A} = \frac{AR_{Ellington}}{2} . \quad \text{(eq. S5)}$$

Replacing wing length and chord by their relative expressions $\hat{r} = r/R$ and $\hat{c} = c/\bar{c}$, the *k*-th moment of wing area is:

$$\begin{aligned} S_{k,Ellington} &= 2\int_0^R cr^k dr \quad \text{(eq. S6)} \\ &= 2\int_0^R \hat{c}\bar{c}(\hat{r}R)^k dr \\ &= 2\int_0^R \bar{c}R^k \hat{c}\hat{r}^k dr \\ &= 2\int_0^R \frac{S_{Ellington}}{2R} R^k \hat{c}\hat{r}^k dr \\ &= S_{Ellington}R^k \int_0^R \hat{c}\hat{r}^k R^{-1} dr . \end{aligned}$$

Considering integration bounds, this equation converts into:

$$S_{k,Ellington} = S_{Ellington}R^k \int_0^1 \hat{c}\hat{r}^k dr . \quad \text{(eq. S7)}$$

The latter equation derives integrated wing area to the power of *k* for each wing blade element along the position *r*. Assuming symmetrical wings on both sides of the animal, we may write the *k*-th moment of area of a single wing as:

$$A_k = \int_0^R cr^k dr = AR^k \int_0^1 \hat{c}\hat{r}^k d\hat{r} = \frac{S_{k,Ellington}}{2} . \quad \text{(eq. S8)}$$

However, due to wing damage, there is no symmetry between left and right wing. This requires to calculate $S = A_L + A_R$ and $S_k = A_{k,L} + A_{k,R}$ with L and R the left and right wing, respectively. Aspect ratio (AR) is thus:

$$AR_{total} = \frac{(R_L + R_R)^2}{A_L + A_R} = \frac{(R_L + R_R)^2}{S} . \quad \text{(eq. S9)}$$

Noteworthy, this approach ignores the body between both wings. Ellington's expression of the non-dimensional *k*-th moment $\hat{r}_k^k$ is equal to:

$$\hat{r}^k_{k,Ellington}(S_{Ellington}) = \frac{S_{k,Ellington}}{S_{Ellington}R^k} = \int_0^1 \hat{c}\hat{r}^k d\hat{r} . \quad \text{(eq. S10)}$$

For a single wing this expression should be written as:

$$\hat{r}_k^k(A) = \frac{A_k}{A \cdot R^k} \int_0^1 \hat{c}\hat{r}^k d\hat{r} = \hat{r}^k_{k,Ellington}(S_{Ellington}) , \quad \text{(eq. S11)}$$

that is identical to Ellington because $\hat{r}_k^k$ is area-independent. The last step is to calculate the non-dimensional radius of the *k*-th moment of wing area, $\hat{r}_k$. According to Ellington, the *k*-th moment of area would be S_k, and the characteristics of the wing planform $\hat{r}_k$ is:

$$\hat{r}_k = \sqrt[k]{\hat{r}_k^k} . \quad \text{(eq. S12)}$$

Supplementary Materials and Methods 7

Similarity of wing damage progression within containers

In the container experiment, flies were kept in groups of four animals and an averaged activity was assigned to each fly. This approach may result in wing damage progression that is more similar in flies from the same group compared to flies from another groups. If flies within a single container are more similar to each other than to other flies, the variance in number of damaged wings, ages at t_{tp}, and logistic fit parameters should be different from randomly assigned pairings. We approached this problem by creating an elevated number of random permutations, shuffling around the flies' group memberships. We tested up to 999 artificial permutations and compared data from the mixed memberships with the data from the measured memberships. For each permutation, we estimated the fraction of damaged wings for all flies with an area loss of more than 15%. A similar procedure we applied to maximum-minimum range of physiological age and logistic parameters (Fig. S5A-H).

To compare the fraction of damaged wings in measured groups with permutated groups, we used a two-sided two-sample Kolmogorov-Smirnov test. We assigned a number to each fly container and ranked them according to the span of ages the flies of each group permutation reached (Fig. S5I). The relative position of the real group was determined. In case of ties, the real group was considered to be in the middle of the tied permutations. If membership does not matter, the ranks should scatter around 0.5. Relative rank was tested by a one-sided *t*-tests on its equality with 0.5 (alternative hypothesis: <0.5). Probability values of Kolmogorov-Smirnov and *t*-tests were also corrected for multiple measurements using Bonferroni correction. In none of the tests, we found any significance between differently grouped memberships (*p*-values for females: 1.00 for fraction of damaged wings, 0.566 for age; males: 1.00 for fraction of damaged wings, 0.168 for age). Data for permutations of logistic fit parameters (analysed in a manner similar to that of age; ranks pooled across parameters of the fits) is shown in figure S5I, J. While medians and arithmetic means were below 0.5 for males, none of the tests showed statistical difference from 0.5. Altogether, the results suggest that group membership has no significance for wing damage patterns in our study.

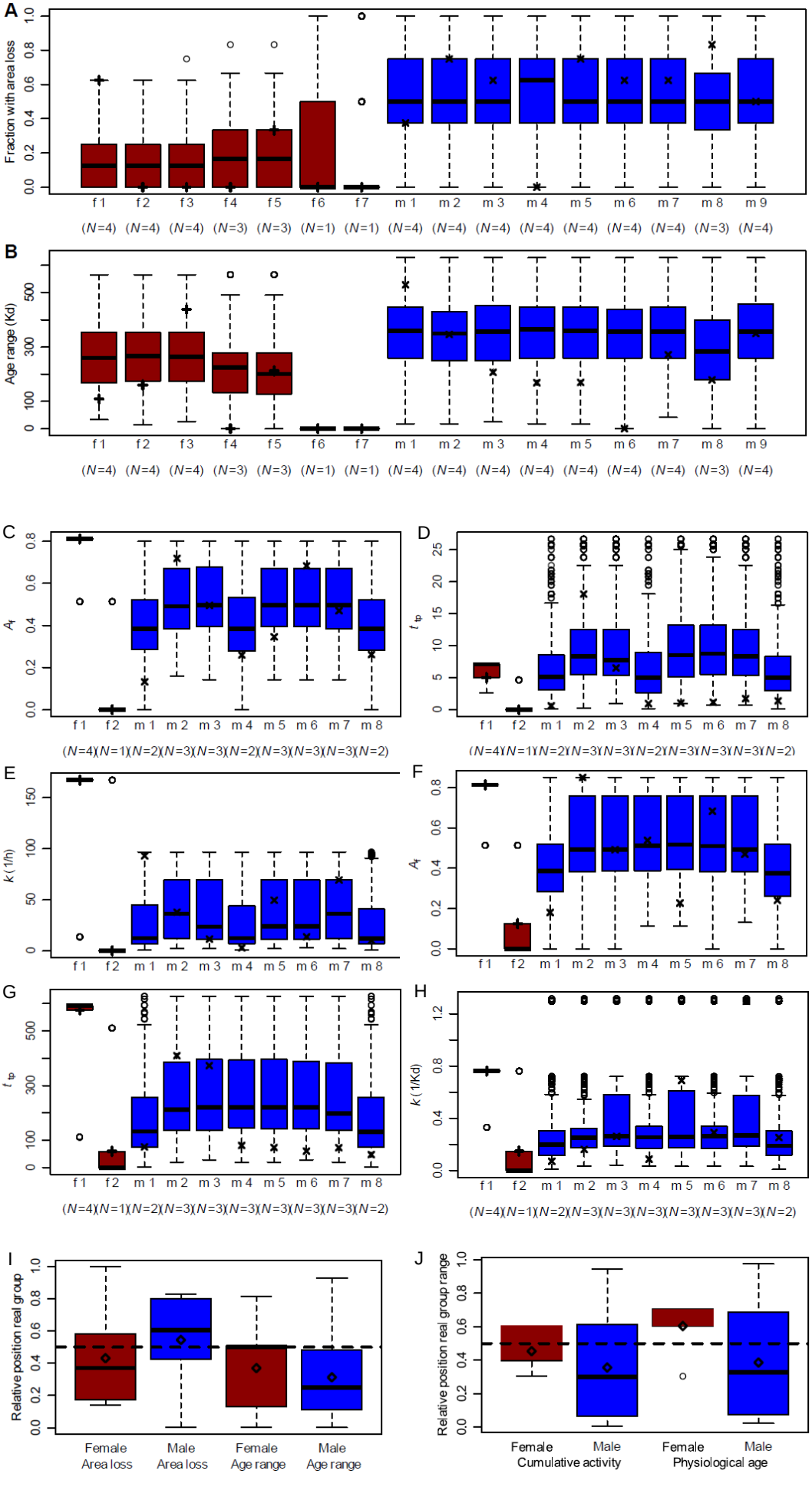
A
Fraction with area loss
f1 f2 f3 f4 f5 f6 f7 m1 m2 m3 m4 m5 m6 m7 m8 m9
(N=4) (N=4) (N=4) (N=3) (N=3) (N=1) (N=1) (N=4) (N=4) (N=4) (N=4) (N=4) (N=4) (N=4) (N=3) (N=4)
B
Age range (Kd)
f1 f2 f3 f4 f5 f6 f7 m1 m2 m3 m4 m5 m6 m7 m8 m9
(N=4) (N=4) (N=4) (N=3) (N=3) (N=1) (N=1) (N=4) (N=4) (N=4) (N=4) (N=4) (N=4) (N=4) (N=3) (N=4)
C
A_f
f1 f2 m1 m2 m3 m4 m5 m6 m7 m8
(N=4)(N=1)(N=2)(N=3)(N=3)(N=2)(N=3)(N=3)(N=3)(N=2)
D
t_{tp}
f1 f2 m1 m2 m3 m4 m5 m6 m7 m8
(N=4)(N=1)(N=2)(N=3)(N=3)(N=2)(N=3)(N=3)(N=3)(N=2)
E
k (1/h)
f1 f2 m1 m2 m3 m4 m5 m6 m7 m8
F
A_f
f1 f2 m1 m2 m3 m4 m5 m6 m7 m8
G
t_{tp}
f1 f2 m1 m2 m3 m4 m5 m6 m7 m8
(N=4)(N=1)(N=2)(N=3)(N=3)(N=3)(N=3)(N=3)(N=3)(N=2)
H
k (1/Kd)
f1 f2 m1 m2 m3 m4 m5 m6 m7 m8
(N=4)(N=1)(N=2)(N=3)(N=3)(N=3)(N=3)(N=3)(N=3)(N=2)
I
Relative position real group
Female Area loss
Male Area loss
Female Age range
Male Age range
J
Relative position real group range
Female Cumulative activity
Male Cumulative activity
Female Physiological age
Male Physiological age

Fig. S5. (A) Relative fraction of wings with wing damage above 15% A_0 loss. (B) Data range (box plot) of physiological age reached by the flies for all permutations (original and permutated groups). Corresponding groups are named "f/m *x*" and correspond to real groups Mf/m*X*, with the number of analysed flies shown below. Circles are outliers and crosses show data range of original group. Red (f) , female groups; blue (m), male groups. (C-E) Cumulative activity of all permutations (original and permutated groups) depicted as box plots. Data range of final relative wing area in *C*, data range of flight activity at the inflexion point of logistic fit in *D*, and data range of logistic growth rate in *E*. Circles are outliers and crosses give the range of the original group (upright for females, tilted for males). (F-H) Data range of physiological age of all permutations (original and artificial groups) depicted as box plots. Data ranges of final relative wing area in *F*, activity at inflexion point of logistic fit in *G*, and logistic growth rate in *H*. (I) Relative rank of fraction of damaged wings and age range of original group compared to all permutations. Data were pooled with respect to group identity. Dashed line at 0.5 indicates no effect of fly group membership. Diamonds, arithmetic means. (J) Relative rank of pooled parameters of successful logistic fits according to cumulative flight activity and physiological age of original group compared with all permutations. Dashed line at 0.5 indicates no effect of fly group membership. Diamonds are arithmetic means.

References

Barthelme, S. (2020). *imager: image processing library based on 'CImg'*. R package version 0.42.3

Chang, W. (2014). *extrafont: Tools for using fonts*. R package version 0.17

Dowle, M. and Srinivasan, A. (2019). *data.table: Extension of 'data.frame'*. R package version 1.12.8

Dunnington, D. and Harvey, P. (2019). *exifr: EXIF image data in R*. R package version 0.3.1

Ellington, C. P. (1984a). The aerodynamics of hovering insect flight. I. The quasi-steady analysis. *Phil. Trans. R. Soc.* B 305(1122), 1–15. doi:10. 1098/rstb.1984.0049

Ellington, C. P. (1984b). The aerodynamics of hovering insect flight. II. Morphological parameters. *Phil. Trans. R. Soc.* B 305(1122), 17–40. doi: 10.1098/rstb.1984.0050

Elzhov, T. V., Mullen, K. M., Spiess, A.-N. and Bolker, B. (2016). *minpack.lm: R Interface to the Levenberg-Marquardt Nonlinear Least-Squares Algorithm Found in MINPACK, Plus Support for Bounds*. R package version 1.2-1

Gagolewski, M. (2020). *R package stringi: Character string processing facilities*

Keitt, T. (2012). *colorRamps: Builds color tables*. R package version 2.3

Komárek, A., Lesaffre, E. and Hilton, J. F. (2005). Accelerated failure time model for arbitrarily censored data with smoothed error distribution. *J. Comp. Graph. Statistics* 14(3), 726–745. doi:10.1198/106186005x63734

Ligges, U., Krey, S., Mersmann, O. and Schnackenberg, S. (2018). *tuneR: Analysis of Music and Speech*

Lisovich, A. and Day, R. (2014). *rChoiceDialogs: rChoiceDialogs collection*. R package version 1.0.6

Mangiafico, S. (2020). *rcompanion: functions to Support Extension Education Program Evaluation*. R package version 2.3.26

McAlpine, J. F. (1981). *Manual of Nearctic Diptera*. Ottawa: Research Branch, Agriculture Canada. ISBN 0660107317

Ooms, J. (2020). *magick: Advanced Graphics and Image-Processing in R*. R package version 2.4.0

Plate, T. and Heiberger, R. (2016). *abind: combine multidimensional arrays*. R package version 1.4-5

R Core Team (2020). *R: A Language and Environment for Statistical Computing*. R Foundation for Statistical Computing, Vienna, Austria

Sarkar, D. (2008). *Lattice: Multivariate Data Visualization with R*. New York

Schindelin, J., Arganda-Carreras, I., Frise, E., Kaynig, V., Longair, M., Pietzsch, T., Preibisch, S., Rueden, C., Saalfeld, S., Schmid, B. et al. (2012). Fiji: an open-source platform for biological-image an alysis. *Nature Methods* 9(7), 676–682. doi:10.1038/nmeth.2019

Skovgård, H. and Nachman, G. (2004). Biological control of house flies *Musca domestica* and stable flies *Stomoxys calcitrans* (Diptera: Muscidae) by means of inundative releases of *Spalangia cameroni* (Hymenoptera: Pteromalidae). *Bulletin of Entomoll Res.* 94(6), 555–567. doi: 10.1079/ber2004322

Urbanek, S. (2013a). *png: Read and write PNG images*. R package version 0.1-7

Urbanek, S. (2013b). *tiff: Read and write TIFF images*. R package version 0.1-5

Urbanek, S. (2019). *jpeg: Read and write JPEG images*. R package version 0.1-8.1

Weis-Fogh, T. (1973). Quick estimates of flight fitness in hovering animals, including novel mechanisms for lift production. *J. Exp. Biol.* 59, 169–230